Available online at www.sciencedirect.com
ScienceDirect
Ceramics International 35 (2009) 1769–1773
CERAMICS INTERNATIONAL
www.elsevier.com/locate/ceramint

Transport properties of $BaCe_{0.85}Y_{0.15}O_{3-\delta}$ at closed-cycle refrigerator temperature

Cheol-Jae Park, Hyun-Wook Ryu, Jong-Ha Moon, Jong-Sook Lee, Sun-Ju Song *

School of Materials Science and Engineering, Chonnam National University, 300 Yongbong-dong, Buk-gu, Gwangju 500-757, South Korea

Received 24 July 2008; received in revised form 6 September 2008; accepted 1 October 2008
Available online 21 October 2008

Abstract

The electrical conducting properties of both hydrated and dehydrated $BaCe_{0.85}Y_{0.15}O_{3-\delta}$ (barium cerate, BCY) were investigated at low temperature (473–203 K) by an AC impedance analyzer combined with a dielectric interface. For the BCY, the bulk and grain boundary conductivities were separated with the equivalent circuit model, and the bulk conductivity was approximately two orders of magnitude higher than the grain boundary conductivity. At very low temperature (203 K), a single semicircle was obtained in the impedance plot, whereas three distinct semicircles were plotted in modulus plot due to the three different resistance components in the system. The activation energy of bulk conductivity was 0.55 eV and 0.57 eV for the hydrated and dehydrated BCY samples, respectively.

Keywords: Proton conductor; $BaCe_{0.85}Y_{0.15}O_{3-\delta}$; Bulk conductivity; Closed-cycle refrigerator

1. Introduction

Since the phenomenon of high-temperature proton conduction in oxides was first reported, acceptor-doped perovskite structures have been intensively studied due to their potential applications for fuel cells, sensors, membranes, and steam electrolyzers [1–3]. Among the perovskites, acceptor-doped barium cerates (BCY: $BaCe_{0.85}Y_{0.15}O_{3-\delta}$) are recognized as the highest proton conductor [4].

Despite its good proton-conducting properties, BCY has not yet been successfully applied for use in electrochemical devices due to its thermodynamic and long-term chemical instability, especially in CO, CO_2, and water-containing conditions [5,6]. Thermal stability was also identified as a major concern when the vapor pressure of BCY was measured by mass spectrometry above 1774 K: BaO(g) was confirmed as the main gas species [7]. Atomistic simulation results [8] showed that the formation of Ba and O vacancy pairs is the most energetically favorable point defect, resulting in the loss of BaO and CeO_2 formation at very high temperature. Loss of BaO from yttrium-doped BCY was believed to be due to either dopant redistribution over the A and B sites or direct evaporation of BaO.

The high-temperature transport properties of acceptor-doped BCY have been intensively studied from conductivity measurements [9], open cell measurements [10], permeation [11], and point defect modeling [12], but their low-temperature properties have not yet received any attention.

In this study, the electrical conducting properties of both hydrated and dehydrated BCY were investigated at low temperature (473–203 K) by an AC impedance analyzer (Solartron 1260) combined with a dielectric interface (Solartron 1296). For the BCY, the bulk and grain boundary conductivities were separated with the equivalent circuit model.

2. Defect chemistry

The defect structure of the system is described by the relations among the structural elements. Mass action laws are applied to defect equilibria and the defect notation of Kroger and Vink [13] is used, in which the subscripts indicate the site, while the superscripts (x), ($^{\bullet}$), and (/) indicate zero, positive,

* Corresponding author. Tel.: +82 62 530 1706; fax: +82 62 530 1699.
E-mail address: song@chonnam.ac.kr (S.-J. Song).

0272-8842/$34.00
doi:10.1016/j.ceramint.2008.10.008

and negative effective charges, respectively. Mass action laws are applied to defect equilibria as follows:

- Internal equilibria:

$$\text{null} = V_{Ba}^{//} + V_{Ce}^{////} + 3V_O^{\bullet\bullet}; \quad K_S = [V_{Ba}^{//}][V_{Ce}^{////}][V_O^{\bullet\bullet}]^3, \tag{1}$$

where K_S is the equilibrium constant for Schottky–Wagner disorder:

$$\text{null} = e^{/} + h^{\bullet}; \qquad K_i = np, \tag{2}$$

where K_i is the equilibrium constant for the electron–hole pair intrinsic reaction.

- External equilibria:

$$\frac{1}{2}O_2(g) + V_O^{\bullet\bullet} \rightarrow O_O^x + 2h; \qquad K_{OX} = p^2[V_O^{\bullet\bullet}]^{-1}P_{O_2}^{-1/2}, \tag{3}$$

where K_{OX} is the equilibrium constant for the oxygen exchange:

$$H_2O(g) + V_O^{\bullet\bullet} + O_O^x \rightarrow 2OH_O^{\bullet}; \qquad K_W = \frac{[OH_O^{\bullet}]^2}{[V_O^{\bullet\bullet}]P_{H_2O}}, \tag{4}$$

where K_W is the equilibrium constant for the water exchange.

- Vaporization equilibrium of BaO:

$$Ba_{Ba}^x + Ce_{Ce}^x + 3O_O^x \rightarrow V_{Ba}^{//} + Ce_{Ce}^x + V_O^{\bullet\bullet} + 2O_O^x + BaO(g); \quad K_B = [V_{Ba}^{//}][V_O^{\bullet\bullet}]a_{BaO}, \tag{5}$$

where K_B is the equilibrium constant for the vaporization of BaO, and a_{BaO} is the activity of BaO.

- Charge neutrality condition:

$$n + 2[V_{Ba}^{//}] + 4[V_{Ti}^{////}] + [Y_{Ce}^{/}] = p + 2[V_O^{\bullet\bullet}] + [OH_O^{\bullet}], \tag{6}$$

The possibility of Frenkel disorder is ruled out because, according to the atomistic simulation, the perovskite structure is highly unlikely to accommodate ion interstitials.

3. Experimental

Polycrystalline BCY powders were prepared by conventional, solid-state reaction methods. High-purity oxide powders of $BaCO_3$ (99.9%, Alfa Aesar), CeO_2 (99.9%, Alfa Aesar), and Y_2O_3 (99.99%, Alfa Aesar) were mixed, ground in a ball mill with stabilized zirconia balls, and calcined at 1523 K for 12 h in air. The calcined oxides were then crushed, sieved through a mesh size of <45 μm, pressed into pellets, cold isostatically pressed, and finally sintered at 1723 K for 12 h in air to afford disks with densities of 96%.

For dehydration, the samples were annealed at 1273 K for 2 h with the Ar gas dried by passing through a column of $CaSO_4$. A wet gas stream produced by bubbling through a water bath at an ambient temperature acted as feed for the hydrating samples at 773 K for 24 h.

The electrical conducting properties of both hydrated and dehydrated BCY were investigated at low temperature (473–203 K, controlled by a closed-cycle refrigerator, CCS-400) by an AC impedance analyzer (Solartron 1260) combined with a dielectric interface (Solartron 1296) over the frequency range of 100 Hz to 100 MHz at an amplitude of 100 mV. Platinum paste (Engelhard 6929) was used as an electrode on both sides of the pellets after their surfaces had been polished.

4. Results and discussion

Fig. 1 shows the scanning electron microscopy (SEM) images of the as-sintered and fractured surfaces. The as-sintered specimen exhibited a porous surface (Fig. 1a) because the chemical evaporation of the component oxide (BaO) caused pore development at the surface of the specimen sintered at elevated temperature. A very dense fractured surface was shown in Fig. 1b. The X-ray diffraction (XRD) spectra on the polished-surface of specimens, shown in Fig. 2, confirm a single-phase perovskite with an orthorhombic structure.

Figs. 3 and 4 show two representative impedance results for both dry and wet conditions, along with the equivalent circuit used in fitting. The impedance response of the BCY samples at 298 K typically showed two semicircles in the Nyquist plot: one small arc at high frequencies, corresponding to the bulk characteristics; and one large arc at medium–low frequencies,

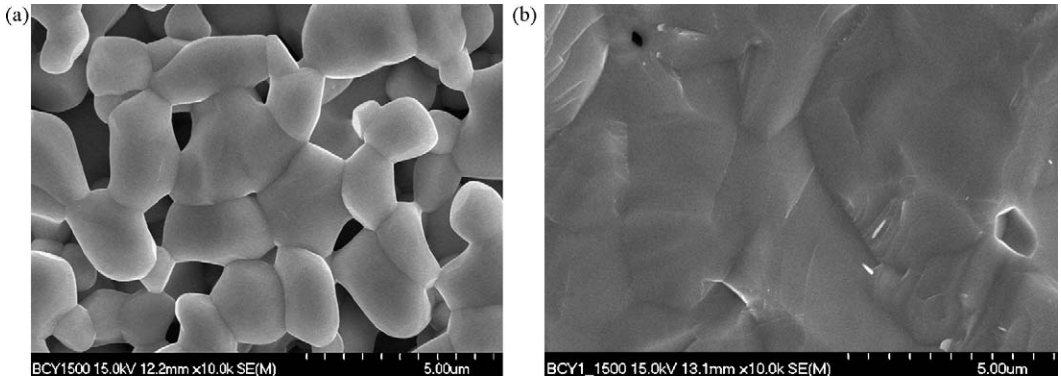

Fig. 1. Scanning electron micrograph (SEM) images of the (a) as-sintered and (b) fractured surfaces of $BaCe_{0.85}Y_{0.15}O_{3-\delta}$ (BCY).

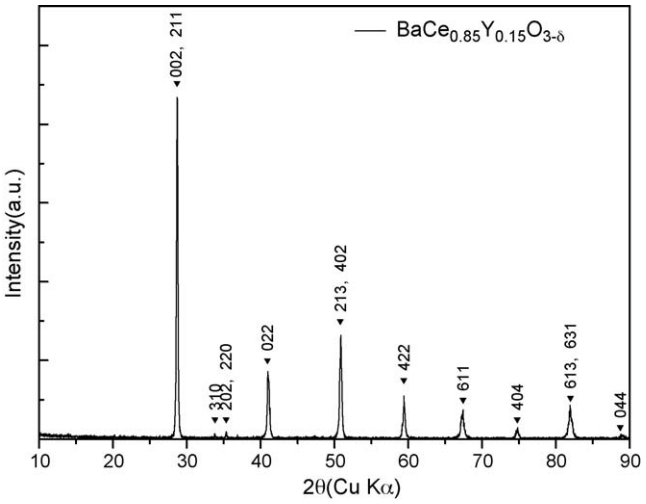

Fig. 2. X-ray diffraction (XRD) patterns of $BaCe_{0.85}Y_{0.15}O_{3-\delta}$ (BCY) sintered at 1673 K in air.

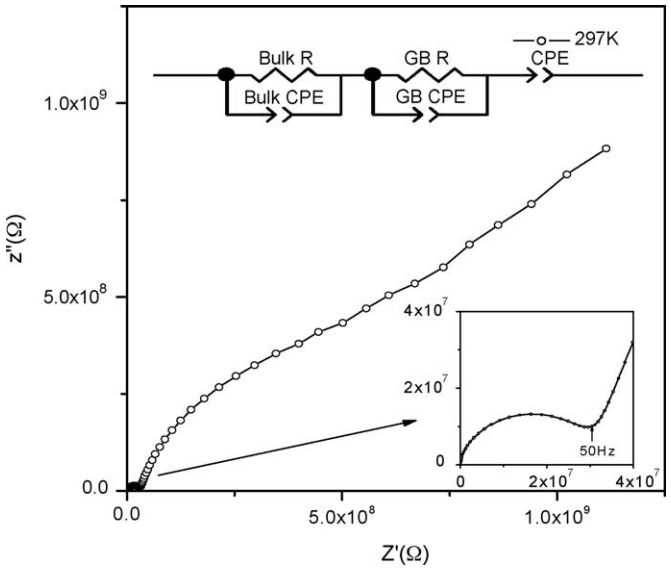

Fig. 4. Typical Nyquist plot of dehydrated $BaCe_{0.85}Y_{0.15}O_{3-\delta}$ (BCY) at around 297 K.

related to both the grain boundary and electrode resistance. The reason how electrode response affects the grain boundary response may be ascribed to the similar resonance frequency of both bulk and grain boundary. In this result, both grain boundary and electrode response was not clearly divided from the medium–low frequency range impedance data, but using equivalent circuit model both terms were successfully separated.

The bulk conductivity was calculated by multiplying the inverse bulk resistance ($1/R_b$) by L/A, where A is the cross sectional area, and L is the thickness of the sample. The bulk and grain boundary resistivities were calculated from impedance measurements by comparing the capacitance of the bulk and grain without further microscopic information, while the bulk and grain boundary dielectric constants were assumed to be approximately equal, as described elsewhere [14,15]. The specific grain boundary conductivity can be calculated from:

$$\sigma_{gb} = \frac{L}{R_{gb}} \frac{\delta_{gb}}{d_g} \tag{7}$$

where R_{gb} is the grain boundary resistance, d_g the grain size, and δ_{gb} is the grain boundary thickness (mainly the thickness of the space charge layer). δ_{gb} may also be calculated from the ratios of the bulk and grain boundary capacitances:

$$\delta_{gb} = \frac{\varepsilon_{gb}}{\varepsilon_b} \frac{C_b}{C_{gb}} d_{gb} \cong \frac{C_b}{C_{gb}} d_{gb} \tag{8}$$

if we approximate the dielectric constant of the grain boundary (ε_{gb}) to the bulk value (ε_b). Although the electrode and grain boundary responses were not clearly divided, we assumed an equivalent circuit of three parallel RC circuits connected in series. The impedance diagrams were fitted to obtain the resistance, characteristic frequency, and capacitance of the bulk, the grain boundary, and the electrodes.

The reported data on the acceptor-doped $BaCeO_{3-\delta}$ show that the concentration of electrons and holes are minor when compared with that of the ionic defects in the higher pO_2 regime

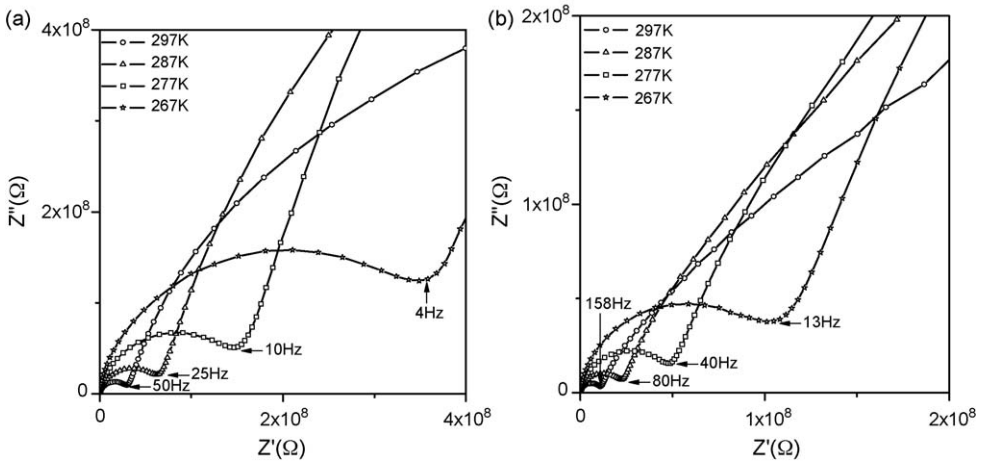

Fig. 3. Nyquist plots at various temperatures for (a) dehydrated and (b) hydrated $BaCe_{0.85}Y_{0.15}O_{3-\delta}$ (BCY).

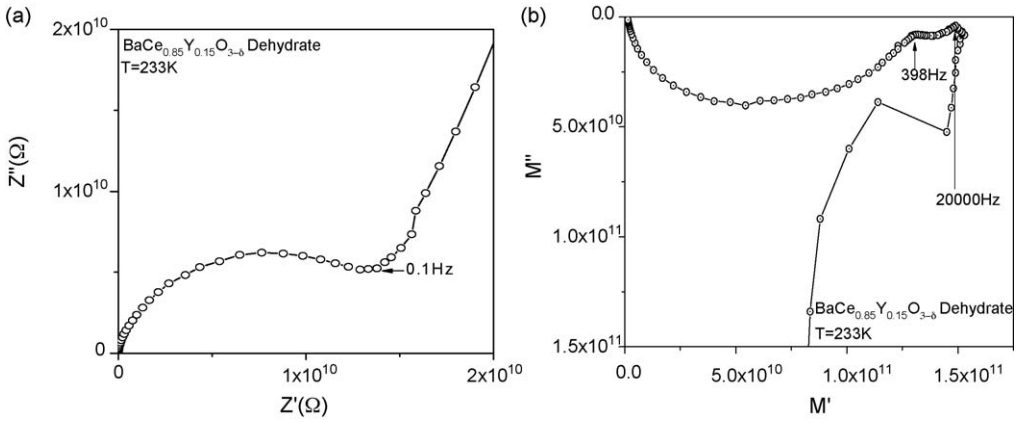

Fig. 5. (a) Impedance and (b) modulus plots at 233 K for dehydrated $BaCe_{0.85}Y_{0.15}O_{3-\delta}$ (BCY).

(N_2/O_2 mixture). Therefore, Eq. (6) simplifies to [16]

$$[Y_{Ce}{}'] = 2[V_O{}^{\bullet\bullet}] + [OH_O{}^{\bullet}] \quad (9)$$

By combining Eq. (1)–(6) and (9), the following defect concentration relationship may be derived

$$[OH_O{}^{\bullet}] = \frac{K_W P_{H_2O}}{4}\left[\left(1+\frac{8[Y_{Ce}{}']}{K_W P_{H_2O}}\right)^{1/2} - 1\right] \quad (10)$$

$$[V_O{}^{\bullet\bullet}] = \frac{K_W P_{H_2O}}{16}\left[\left(1+\frac{8[Y_{Ce}{}']}{K_W P_{H_2O}}\right)^{1/2} - 1\right]^2 \quad (11)$$

$$p = \left(\frac{K_{OX}K_W}{16}\right)^{1/2} P_{O_2}^{1/4} P_{H_2O}^{1/2}\left[\left(1+\frac{8[Y_{Ce}{}']}{K_W P_{H_2O}}\right)^{1/2} - 1\right] \quad (12)$$

Though an oxygen vacancy is a major positive charged defect, it is evident that the hole conduction is dominant in the p-type regime, because a higher total conductivity was reported at the dry oxygen condition than at the dry argon condition.

In the case of the wet argon condition, a proton may be incorporated into BCY by consuming the oxygen vacancy, as shown in Eq. (4), and further be dissolved according to the following equation:

$$H_2O(g) + 2h^{\bullet} + 2O_O{}^{x} \rightarrow 2OH_O{}^{\bullet} + \frac{1}{2}O_2(g) \quad (13)$$

As shown in a previous simulation work [12], proton incorporation increases with both decreasing oxygen partial pressure (pO_2) at a fixed water vapor pressure and increasing water partial pressure (pH_2O) at a fixed pO_2. Therefore, proton conduction becomes dominant at the wet argon condition.

Comparing the impedance diagrams for both dry- and wet-BCY disk samples indicated that the medium frequency semicircle (associated with grain boundary resistance) was larger for the wet-BCY disk, indicating that BCY has a larger

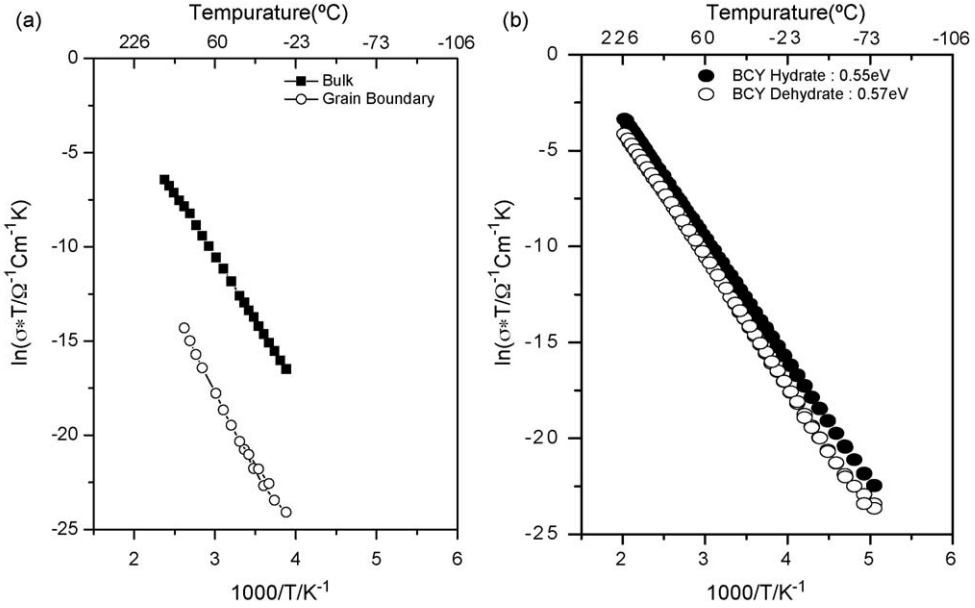

Fig. 6. (a) Arrhenius plots of bulk and grain boundary conductivity of dehydrated $BaCe_{0.85}Y_{0.15}O_{3-\delta}$ (BCY), and (b) temperature dependence of total conductivity for dehydrated and hydrated BCY.

grain-boundary resistance at the dry condition (grain boundary resistance: 5.93×10^8, shape factor: 0.22 at 297 K) than at the wet condition (grain boundary resistance: 7.59×10^7, shape factor: 0.257 at 297 K).

At low temperature (up to 243 K), there is only a single overlapped arc at intermediate frequencies, together with the beginning an arc at low frequencies assigned to the electrode response. Due to the similar capacitance of the bulk/grain boundary at the temperature studied, the overlapped arc could not be further analyzed. In Fig. 5, the electrical response of the bulk and grain boundaries was successfully resolved in the modulus spectrum because of the difference in their resistance.

The Arrhenius plot of the electrical conductivity is shown in Fig. 6. The bulk conductivity was several orders of magnitude higher than the grain boundary conductivity over the temperature range of 473–203 K for dehydrated BCY. This result confirmed that the grain boundary may not provide a pathway for fast proton transport, and that bulk transport makes a major contribution to the total conductivity [17]. The calculated activation energy, consisting of the formation and migration energy for mobile defect species, was 0.55 eV and 0.57 eV for the hydrated and dehydrated BCY samples, respectively.

5. Conclusion

The electrical conducting properties of both hydrated and dehydrated BCY were investigated at low temperature (473–203 K) by an AC impedance analyzer combined with a dielectric interface. For the BCY, the bulk and grain boundary conductivities were separated with the brick-layer model, and the bulk conductivity was approximately two orders of magnitude higher than the grain boundary conductivity. The activation energy of bulk conductivity for the hydrated BCY was 0.55 eV and 0.57 eV for the hydrated and dehydrated BCY samples, respectively.

Acknowledgements

This work was supported by a Korea Research Foundation Grant funded by the Korean Government (MOEHRD, Basic Research Promotion Fund) (KRF-2007-331-D00199).

References

[1] H. Iwahara, Y. Asakura, K. Katahira, M. Tanaka, Solid State Ionics 168 (2004) 299–310.
[2] W.G. Coors, J. Electrochem. Soc. 151 (7) (2004) A994–A997.
[3] S.-J. Song, E.D. Wachsman, J. Rhodes, S.E. Dorris, U. Balachandran, Solid State Ionics 167 (2004) 99–105.
[4] K.D. Kreuer, Solid State Ionics 125 (1999) 285–302.
[5] K.-H. Ryu, S. Haile, Solid State Ionics 125 (1999) 355–367.
[6] K.D. Kreuer, Solid State Ionics 97 (1997) 1–15.
[7] J. Wu, L.P. Li, W.T.P. Espinosa, S.M. Haile, J. Mater. Res. 19 (8) (2005) 2366–2376.
[8] J. Wu, R.A. Davies, M.S. Islam, S.M. Haile, Chem. Mater. 17 (2005) 846–851.
[9] S.-J. Song, E.D. Wachsman, S.E. Dorris, U. Balachandran, J. Electrochem. Soc. 150 (2003) A1484–A1490.
[10] H. Iwahara, H. Uchida, K. Ono, K. Ogaki, J. Electrochem. Soc. 135 (2) (1988) 529–533.
[11] S.-J. Song, E.D. Wachsman, J. Rhodes, S.E. Dorris, U. Balachandran, Solid State Ionics 164 (2003) 107–116.
[12] S.-J. Song, E.D. Wachsman, S.E. Dorris, U. Balachandran, Solid State Ionics 149 (2002) 1–10.
[13] F.A. Kroger, V.J. Vink, in: D. Turnbull (Ed.), Relations between the Concentrations of Imperfections in Crystalline Solids, Solid State Physics, vol. 3, Academic Press, New York, 1956, pp. 307–435.
[14] S.M. Haile, D.L. West, J. Campbell, J. Mater. Res. 13 (1998) 1576–1595.
[15] J.R. Macdonald, Impedance Spectroscopy, John Wiley & Sons, New York, 1987.
[16] S.-J. Song, E.D. Wachsman, S.E. Dorris, U. Balachandran, J. Electrochem. Soc. 150 (2003) A790–A795.
[17] S.-J. Song, J.-H. Moon, T.-H. Lee, S.E. Dorris, U. Balachandran, J. Ceram. Process. Res. 9 (4) (2008) 376–380.